Osteoarthritis and Cartilage 22 (2014) 1053–1060

Osteoarthritis and Cartilage

OARSI OSTEOARTHRITIS RESEARCH SOCIETY INTERNATIONAL

The role of endplate poromechanical properties on the nutrient availability in the intervertebral disc

A. Malandrino †, D. Lacroix ‡, C. Hellmich §, K. Ito ||, S.J. Ferguson ¶, J. Noailly † *

† *Biomechanics and Mechanobiology, Institute for Bioengineering of Catalonia, Barcelona, Spain*
‡ *INSIGNEO Institute for in silico Medicine, Department of Mechanical Engineering, University of Sheffield, Sheffield, UK*
§ *Institute for Mechanics of Materials and Structures, Vienna University of Technology, Vienna, Austria*
|| *Orthopedic Biomechanics, Department of Biomedical Engineering, Eindhoven University of Technology, Eindhoven, The Netherlands*
¶ *Institute for Biomechanics, ETH, Zurich, Switzerland*

ARTICLE INFO

Article history:
Received 15 November 2013
Accepted 7 May 2014

Keywords:
Bony endplate
Spine mechanobiology
Intervertebral disc metabolites
Hydraulic permeability
Bone porosity
Poromechanics

SUMMARY

Objective: To investigate the relevance of the human vertebral endplate poromechanics on the fluid and metabolic transport from and to the intervertebral disc (IVD) based on educated estimations of the poromechanical parameter values of the bony endplate (BEP).
Methods: 50 micro-models of different BEP samples were generated from μCTs of lumbar vertebrae and allowed direct determination of porosity values. Permeability values were calculated by using the micro-models, through the simulation of permeation via computational fluid dynamics. These educated ranges of porosity and permeability values were used as inputs for mechano-transport simulations to assess their effect on both the distributions of metabolites within an IVD model and the poromechanical calculations within the cartilaginous part of the endplate i.e., the cartilage endplate (CEP).
Results: BEP effective permeability was highly correlated to local variations of porosity ($R^2 \approx 0.88$). Universal patterns between bone volume fraction and permeability arose from these results and from other experimental data in the literature. These variations in BEP permeability and porosity had negligible effects on the distributions of metabolites within the disc. In the CEP, the variability of the poromechanical properties of the BEP did not affect the predicted consolidation but induced higher fluid velocities.
Conclusions: The present paper provides the first sets of thoroughly identified BEP parameter values that can be further used in patient-specific poromechanical studies. Representing BEP structural changes through variations in poromechanical properties did not affect the diffusion of metabolites. However, attention might be paid to alterations in fluid velocities and cell mechano-sensing within the CEP.

Introduction

The endplate is an osteochondral spinal structure as thin as approximately 1 mm that has long been recognized as a fundamental component in human intervertebral disc (IVD) biomechanics and mechanobiology, and in the pathophysiology of the IVD degeneration[1]. It is a specialized tissue at the interface between the vertebrae and the cartilaginous IVD[2], being composed by an osseous layer – the bony endplate (BEP) – and a hyaline cartilage layer – the cartilage endplate (CEP).

CEP poromechanics has been suggested to control the fluid exchanges between discs and vertebrae in a direction-dependent manner—i.e., cranially or caudally—, being responsible for the functional balance between diurnal and night changes in IVD volume and height[3,4]. *In silico* studies (i.e., through computer simulations) have confirmed that fluid pressures and velocities and matrix consolidation in the disc are highly affected by the hydraulic CEP permeability[5], much lower than that of the BEP. The cranio-caudal pathway through the endplates is also relevant with regard to the diffusion of essential solutes, i.e., oxygen, glucose and lactate[6]. Capillary buds located in the BEP—but not penetrating the CEP—carry the aforementioned solutes that regulate cell metabolism in the avascular disc. Thus, both the density of bud openings and the porosity (i.e., fluid volume fraction) of the endplate subtissues have been investigated in relation to disc degeneration[7], in

* Address correspondence and reprint requests to: J. Noailly, Biomechanics and Mechanobiology, Institute for Bioengineering of Catalonia, Baldiri Reixac, 4-8, 08028 Barcelona, Spain. Tel: 34-934020266.
E-mail address: jnoailly@ibecbarcelona.eu (J. Noailly).

http://dx.doi.org/10.1016/j.joca.2014.05.005
1063-4584/

turn relevant to low back pain[8]. Organ cultures have also highlighted the importance of the whole endplate (CEP and BEP) poromechanical and transport properties: the CEP contains the aggrecans of the nucleus pulposus (NP), helping to maintain the IVD hydration, and a proper clearing of the marrow space in the BEP can better guarantee a suitable cell viability *in vitro* after 1 week[9].

However, relevant features of the *human* endplates on the IVD mechanobiology are still controversial. During ageing and/or degeneration, CEP calcification and BEP sclerosis have been reported: markers of hypertrophic chondrocytes, involved in calcification[10], and remarkable mineralization have been observed in mature human CEPs[11,12]. Intense CEP calcification in scoliotic discs[6], decreased permeability of the BEP–CEP in degenerated human discs[13], and disturbances in solute diffusion in early degenerated human discs[14] have been observed as well. It has been postulated that nutrient flow may be hindered by tissue sclerosis or calcification, contributing to disc degeneration[7,15]. No objective study has explored, however, how these endplate structural changes would affect both nutrient and fluid exchanges, once they are translated into changes in BEP porosity and hydraulic permeability. This knowledge would contribute to a more mechanistic view about the role of the endplate in IVD maintenance and degeneration.

Recent permeation studies have shown that the hydraulic permeability of human endplates is much higher than previously measured for other species and can increase with age or degeneration[16]. BEP porosity also increases with age and degeneration, contrasting with the idea that nutrient diffusion can be interrupted by BEP sclerosis[16,17]. However, these phenomena could be biased by the fact that advanced degeneration can be concomitant with increased amounts of endplate fissures, causing a rise in the effective porosity and permeability[17]. Also, by analyzing micro computer tomography (μCT) images, disc degeneration has been associated to thicker BEPs but with lower bone mineral density (BMD), pointing out that sclerosis, previously associated to increased BMD[18], might not be linked to disc degeneration in humans[19]. These image-based quantifications are a valuable tool together with permeation experiments on endplate samples. However, the latter may lack robustness due to the extremely reduced BEP thickness and to the difficulty in separating the respective effects of the osseous and cartilaginous regions, especially when calcified CEP tissue binds to the BEP and occludes the bud openings[20]. Improper control of the sealing of the specimen perimeter may also allow peripheral flow due to the high CEP hydraulic resistance, which may alter permeability measurements.

Because μCT provides with bone structural mapping for the BEP region, when converted into a three-dimensional model, this mapping allows evaluating the resistance of the structure to fluid flow through simulated permeation. Thus, the present study aimed at a protocol that quantifies the BEP poromechanical parameters, such as porosity and permeability, through the integration of μCT image processing and permeation through computational fluid dynamics (CFD). Resulting BEP poromechanical parameters were further used as input data for *in silico* explorations of disc poromechanical response and metabolic transport, providing with educated extrapolations to the influence of BEP structure on disc mechanobiology.

Materials and methods

μCT scans of central BEPs from nine human lumbar vertebrae from five subjects were used [Fig. 1(a)]. The age of the donors ranged 64–85 and the degeneration grade was known for six out of twelve discs adjacent to the BEPs studied, being either three or four on the Thompson scale. Acquisitions had been performed previously[7,21] at two different voxel resolutions (12 and 16 μm). In order to have at least three measurements per vertebra, a total of 50 3D parallelepiped samples (~$2.5 \times 2.5 \times 3.5$ mm^3) were modelled for CFD analyses. The models were cropped and segmented from a region of interest (ROI) in the central BEP of each vertebra [Fig. 1(a)], and their squared sub-region (~2.5×2.5 mm^2) was perpendicular to the cranial-caudal direction, aligned with the fluid flow direction [Fig. 1(a) and (b)]. The dimensions of the parallelepipeds were selected so as to translate the local porosity and permeability values into a millimetre-level homogenized continuum, for subsequent use in the mechano-transport simulations. Due to the difficulty to extract visually the densest bone layer, i.e., the functional BEP, some trabecular bone was left for CFD analyses [Fig. 1(b)], the thickness of these trabecular regions plus the attached BEPs being approximately 1.5 mm. A mesh convergence study guaranteed that pressures were not dependent on the final mesh refinement [shown in Fig. 1(c)], which in turn was not dependent on the voxel resolution. BEP permeation was simulated as follows: a mass flux of 10^{-5} kg s^{-1} was applied at the inlet, i.e., at approximately 2 mm from the bone (trabecular plus BEP) [Fig. 1(d)] to stabilize the upstream pressure. Mass flux of this magnitude occurs under normal physiological conditions[4], and lies in the laminar regime. The pressure at the outlet surface was null and "no-slip" conditions were imposed on the other surfaces. These boundary conditions ensured the proper simulation of the pressure rise in a permeation experiment, i.e., avoiding any outflow other than at the outlet. The macroscopic permeability was evaluated by using the Darcy relation:

$$k_0 = \frac{\mu Q_{\text{in}} L}{\rho A (P_{\text{in}} - P_{\text{out}})} \tag{1}$$

being k_0 the intrinsic permeability, Q_{in} the inlet mass flux, A the transversal cross-section, μ and ρ the fluid dynamic viscosity and density, respectively, and L the distance between the two sections characterized by the pressures P_{in} and P_{out} [Fig. 1(d)]. The effective value for L on each sample corresponded to a functional thickness, determined as follows: the depth of the bone within each parallelepiped sample was divided into 50 equidistant points. An average pressure was calculated in each of the 50 corresponding cross-sections in order to obtain a complete profile of pressure drop within the bone sample, in the flow direction. Pressure was then plotted against the axial distance, and because the densest bone layers are expected to generate the largest pressure gradients, the curve slope variations gave an estimation of this BEP functional thickness L (see results, Fig. 2) from which intrinsic permeability was then computed.

For the densest regions of each sample, we also evaluated (1) the porosity ϕ_0 by dividing the fluid volume segmented within the BEP by the total volume of the BEP structure, and (2) the specific surface S_v. The latter was determined either from the 3D reconstructions, by dividing the solid bone surface by the total volume, or as a function of porosity, by using the empirical relationship[22]:

$$S_v = 32.3\phi_0 - 93.9\phi_0^2 + 134\phi_0^3 - 101\phi_0^4 + 28.8\phi_0^5 \tag{2}$$

Standard power-law correlations between porosity and intrinsic permeability values were compared in terms of coefficient of determination R^2 for (1) the 50 samples assuming independence, and for these values grouped (2) by vertebra, and (3) by subject. For all data ungrouped, a porosity-permeability Kozeny–Carman model was also used[23]:

$$k_0 = c\frac{\phi_0^\alpha}{S_v^2}, \tag{3}$$

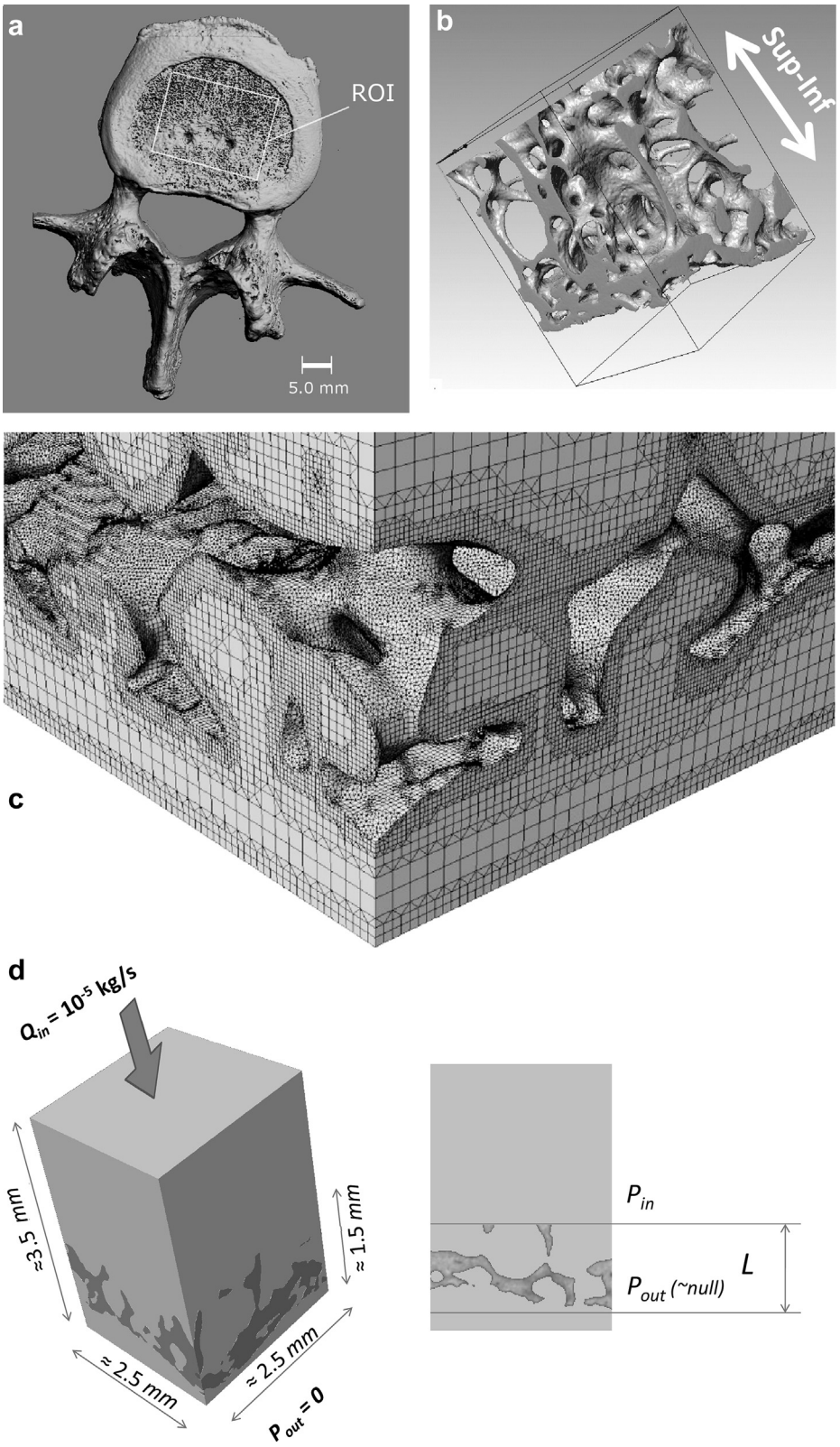

Fig. 1. BEP samples. a) Localization within the central ROI of the vertebra. b) CT scan-based reconstruction and c) CFD mesh modelling. d) Final CFD 3D configuration and planar projection of the simulation conditions for the permeability calculation.

where c and α are correlation coefficients. Eq. (3) has an acceptable asymptotic behaviour for $\phi_0 \approx 0$ and $\phi_0 \approx 1$ thanks to the presence of S_v at the denominator[23]. For the model reconstruction and the CFD analyses, the software ScanIP© (Simpleware Ltd.) and FLUENT© (ANSYS) were used, respectively. Additionally, unpaired t-test was performed to analyse the differences between BEPs adjacent to discs with different degeneration grades (grade 3 $N = 16$ and grade 4 $N = 6$).

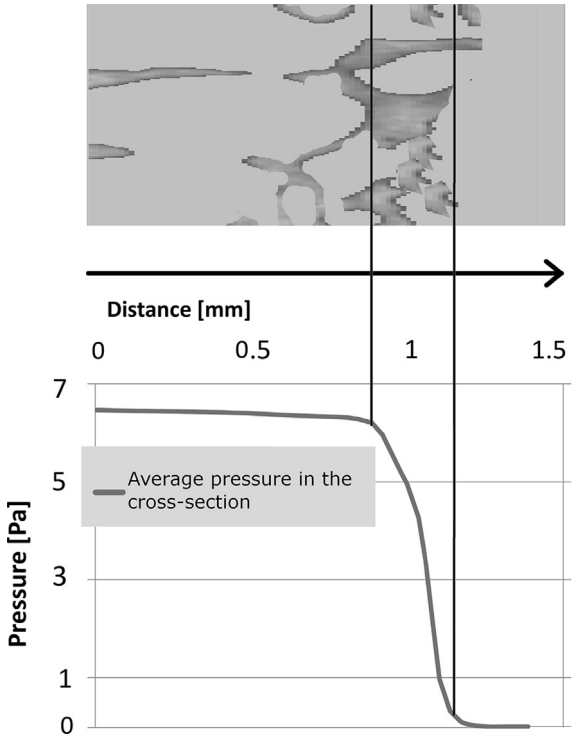

Fig. 2. Plot of the average pressure along the direction of the flow across one of the specimens tested. The BEP functional thickness is delimited by the vertical light grey lines (change in pressure slope), where hydraulic resistance is evaluated.

From the above CFD study, ranges of values were obtained for both the porosity and the permeability of the BEP. The extreme values of these ranges of porosity and permeability were used to explore the possible influence of extreme BEP structural variations on the oxygen and lactate concentrations within the IVD through a finite element poromechanical model coupled with diffusion, advection, reaction, and cell viability[24,25] (see also Supplementary text for the methodological details). Given that BEP porosity and BEP permeability were highly correlated (see Results), they were varied together to produce two mechano-transport model cases: (a) low BEP porosity and permeability and (b) high BEP porosity and permeability (see Supplementary text as well as results of the CFD study for the parameter values). 2 days of mechano-transport were simulated. Each day consisted in a sustained compression (16 h, 0.5 MPa) followed by a resting phase (8 h, 0.1 MPa). In order to assess the effect of the BEP poromechanical parameters on the poromechanical response of the adjacent CEP, the distributions of CEP porosities and fluid velocities obtained for the aforementioned cases (a) and (b) were compared to each other.

Results

A characteristic pressure–distance plot through the axial direction for one of the specimens studied is shown in Fig. 2. The change of slope used for the estimation of the functional thickness and permeability is also visible. The functional thickness, averaged over the 50 samples, was 0.46 ± 0.28 mm, and was not correlated to porosity or to permeability, appearing thus as an independent, morphology-related intrinsic property. BEPs adjacent to grade 3 and grade 4 discs did not statistically differ in either porosity ($P = 0.56$) or permeability ($P = 0.98$). The calculated intrinsic permeability values ranged from 2.60×10^{-14} to 1.81×10^{-9} m^2 (i.e. from 2.6×10^{-11} to 1.81×10^{-6} m^4/Ns in terms of hydraulic permeability obtained dividing by the dynamic viscosity of water), and the porosity values from 11% to 81%. A positive power-law correlation ($R^2 = 0.88$) was found between the permeability and porosity values pooled for all samples [Fig. 3]. Estimation of the specific surface, either from the 3D reconstructions or from Eq. (2), and further use of the Kozeny–Carman model (Eq. (3) and Fig. 3) always led to similar results and reasonable correlation coefficients, i.e., $R^2 = 0.86$, and $R^2 = 0.87$, respectively. Porosity and permeability values are reported in Table I, per subject and vertebra.

Grouping these results per vertebra or per subject led to permeability–porosity correlations similar to those achieved when samples were ungrouped (considered independent). Correlation coefficients (power law) ranged from 0.93 (grouped per vertebra, Fig. 3), to 0.99 (grouped per subject, curve not shown). Accordingly, the porosity and permeability data obtained in the present study followed a "universal" relationship between solid volume fraction ($=1 - \phi_0$) and permeability, when pooled with other experimental measurements [Fig. 4][16,26–29].

When the extreme high and low BEP porosity/permeability values were inserted into the mechano-transport model, relative differences lower than 1% were computed over time in terms of oxygen and lactate concentrations within the IVD.

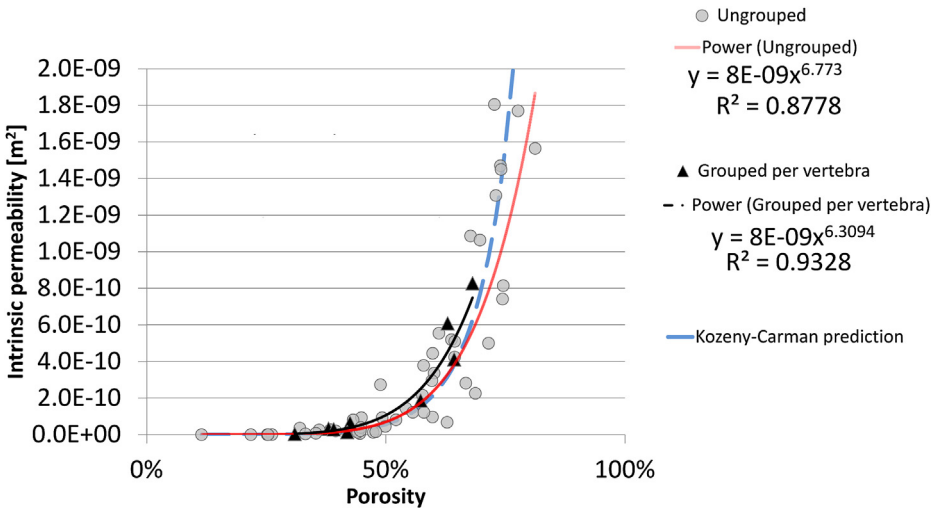

Fig. 3. Power-law fit between BEP permeability and porosity for the samples both ungrouped ($N_{samples} = 50$), and grouped per vertebra ($N_{vertebra} = 9$), and representation of the Kozeny–Carman model fit.

Table I
Porosity and intrinsic permeability and results averaged by vertebra (VERT) with the corresponding standard deviation (SD) and the number of samples (*N*). The subject is also indicated (Subj)

	Subj #1*				Subj #2*		Subj #3		Subj #4		Subj #5
	VERT#1 ($N = 3$)	VERT#2 ($N = 3$)	VERT#3 ($N = 3$)	VERT#4 ($N = 3$)	VERT#5 ($N = 7$)	VERT#6 ($N = 3$)	VERT#7 ($N = 5$)	VERT#8 ($N = 13$)	VERT#9 ($N = 10$)
Mean porosity ± SD [%]	0.573 ± 0.028	0.643 ± 0.069	0.425 ± 0.027	0.419 ± 0.077	0.380 ± 0.117	0.391 ± 0.095	0.309 ± 0.149	0.681 ± 0.081	0.629 ± 0.095
Mean intrinsic permeability ± SD [m^2]	1.87E-10 ± 9.43E-11	4.12E-10 ± 1.70E-10	6.47E-11 ± 3.91E-11	1.39E-11 ± 8.84E-12	3.26E-11 ± 4.21E-11	2.96E-11 ± 1.95E-11	3.87E-12 ± 5.54E-12	8.28E-10 ± 6.50E-10	6.08E-10 ± 4.82E-10

* For these subjects the degeneration grade of adjacent discs was known.

Porosity calculations over time in the CEP were not affected by the extremely high and low BEP porosity/permeability values, and current CEP porosity was always close to the initial value of 80%. Fluid velocities within the CEP were always lower than 3.0–3.5 μm/s. These maximum values were computed just after the application and the removal of the diurnal load. These CEP fluid velocity distributions for the two cases of BEP poromechanical parameters are shown as colour plots in Fig. 5(a) and as histograms in Fig. 5(b). Histograms show that although for the two cases of porosity and permeability of the BEP the mean values of velocities in the CEP are similar, the range of these values is larger for low values of BEP porosity and permeability. In the latter case, higher velocities can be reached for approx. 10% of CEP finite elements during both loading and unloading phases.

Discussion

In the present study, we determined BEP porosity and permeability values based on the three-dimensional information of the bone structure. We further used a mechano-transport poromechanical disc model in order to address the influence of these parameters on both the metabolic transport within the IVD and the CEP poromechanics.

The ranges of BEP porosity and permeability values obtained were very large. Permeability values covered part of the ranges previously measured for both trabecular (2.68×10^{-11}–2.00×10^{-8} m^2)[29] and cortical bones (5×10^{-15}–6.35×10^{-13} m^2)[23]. BEP can be denser than trabecular bone and have a similar microstructure, naturally leading to lower porosity and permeability values at the millimetre scale. Nevertheless, part of the porosity determined in the present study may be due to the space left by the bone marrow contact channels. These channels are specialized for the vertebrae-discs exchange of metabolites[7] and whether they subtract space for fluid flow, thus affecting the effective permeability of the BEP *in vivo*, is not clear. The difference between BEP and cortical bone may be more difficult to interpret because BEP lacks of Haversian structures and the permeation mechanism might be different from those happening in the trabecular bone. Nevertheless, our data and correlations could be the basis for future micromechanics-based explorations[30] to clarify these points. As for structural defects, fissures in the BEP would only modify the effective porosity and permeability of the BEP, leading to an extensive range of local values. The effect of such an extensive range is provided by our study at the tissue and organ level.

Unfortunately, the available information about the donors was insufficient to correlate BEP poromechanics with IVD degeneration grades other than grade 3–4. Hence, our study cannot infer that BEP poromechanical properties and disc degeneration are linked to each other statistically. Such an issue suggests that the high heterogeneity of a single BEP already induced a strong variability of local structures, and porosity and permeability values among the different samples. This variability is probably largely sufficient to already cover the inter-individual, inter-level, or degeneration-dependent differences expected. However, both a positive porosity–permeability correlation and a valid permeability predictor in the form of a Kozeny–Carman model were derived. The porosity–permeability correlation in the BEP seemed robust and universal because: (1) it was not biased by the residual presence of the CEP (not visible in tomographic images) and (2) was confirmed through the use of BEP samples with a large structural diversity, independently on whether data were clustered per donor or per vertebra. The correlation of Fig. 4 further shows universality for several types of bones. Such universal trends throughout different bone tissues have been evidenced also for composition and

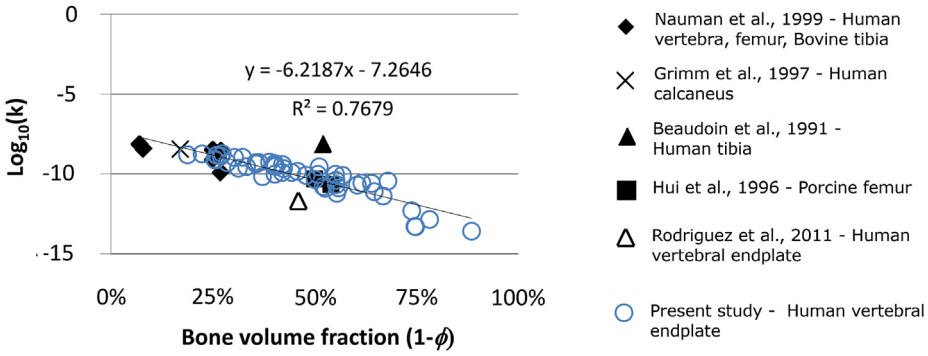

Fig. 4. Variation of the logarithm of the BEP permeability with the solid volume fraction of the BEP, and comparison with other bone measurements in the literature.

mechanical properties[31], and are relevant for parametric studies aiming at exploring the relation between bone structure in several conditions (e.g., sclerosis, osteoporosis) with IVD degeneration.

In the present study no effective difference in models built at 12 and 16 μm voxel size was noted. Although the correlation between porosity and permeability calculated from Eq. (3) was valid when using specific surface values obtained from the 3D reconstructions, we preferred to use Eq. (2), since it is more general and free from segmentation-related issues. With such S_v calculations, fitting our data to Eq. (3) gave $c = 0.079$ and $\alpha = 6.44$, which can be used to predict BEP permeability from porosity (blue line in Fig. 3). By exploiting the association between local porosity values and attenuation coefficients of clinical CT images[32], these correlations can predict the tissue permeability at the voxel level with minimal additional information on the microstructure[33], and could be used to guide multiscale homogenized bone models[30,31].

When used as input in our mechano-transport model, the extreme values of the ranges of BEP porosity and permeability did not affect the calculations of the oxygen and lactate concentrations that are volume changes-dependent[24]. Hence BEP morphological changes do not seem to be responsible alone for the dehydration of the disc (i.e., volume changes). Thus, in contrast to other species[18] and to speculations on human discs[6], our results strongly suggest that BEP sclerosis in humans does not contribute to disc degeneration[16,19]. Yet, future developments should specifically target the porosity related to the bone marrow contact channels[7]. As discussed earlier, our correlations of BEP poromechanical properties could be the basis of such developments, in order to eventually

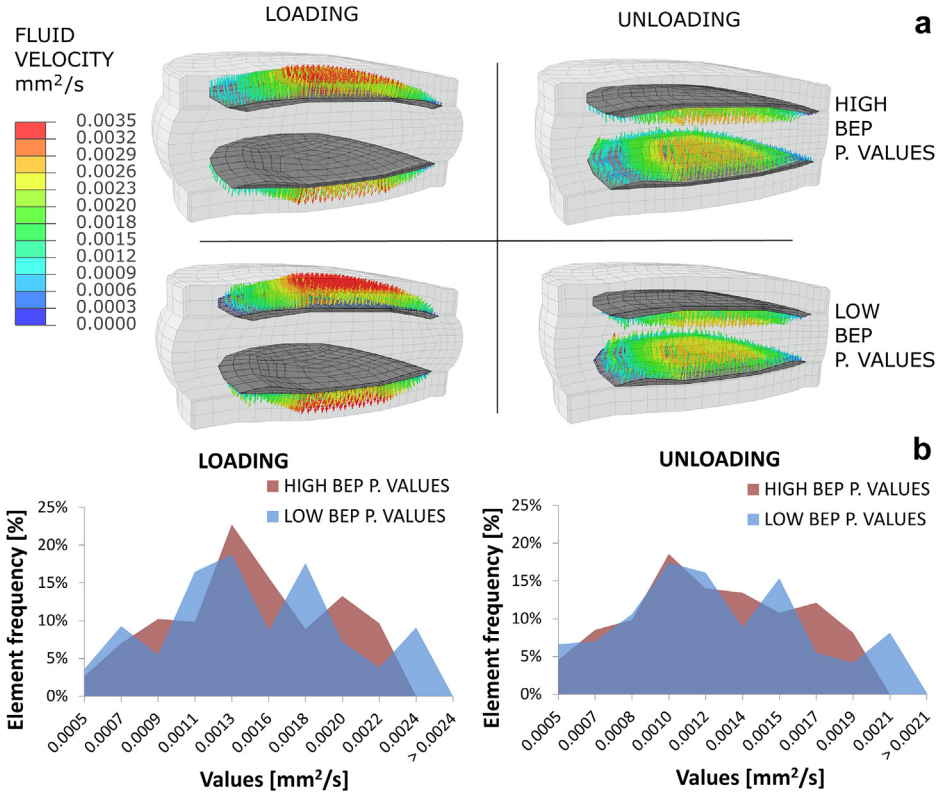

Fig. 5. Fluid velocity distribution within the CEP with the two cases of extreme BEP poromechanical values (high and low) found in the present study, under high-rate mechanical loading and unloading. a) Plots of CEP fluid velocity (arrows) mapped onto the FE mesh used and b) histogram of CEP fluid velocity calculated at the centroids of the elements. The *x*-axis shows ranges of velocities, and *y*-axis shows the corresponding (to each range) percentage of elements.

obtain personalized boundary solute concentration as a function of endplate calcification.

Numerous *in silico* explorations have revealed the likely importance of the CEP in controlling the disc mechanical behaviour and the cell survival[4,5,7,34]. Hence it appears also important to relate the poromechanical characteristic of the BEP to the CEP poromechanics. It has been shown that the permeability and the porosity of the CEP affect very differently the disc mechano-transport. In a previous numerical study[24], we have demonstrated that varying the CEP hydraulic permeability over one order of magnitude resulted in negligible changes in solute concentrations. Yet CEP porosity variations have been shown to have a remarkable influence on cell viability[34–36], correlating with nutritional deficiencies that were suggested to occur along CEP calcification[37]. Indeed, the CEP is not vascularised: thus a drop in its fluid content (porosity) is responsible for a reduced movement of solutes within the fluid (drop of diffusivity). According to the mechano-transport results obtained in this study, changing the poromechanical parameters in the BEP did not affect the porosity changes in the CEP over cycles of daily mechanical loads. However, our calculations revealed that low BEP poromechanical values could induce higher velocities in some CEP regions, in both rapid loading and unloading regimes. Intuitively, this outcome suggests that lower BEP permeability and porosity values contribute to increase the pressure gradients throughout the vertebral endplate which naturally results in higher fluid velocities within the adjacent CEP region (approx. 10%). Nevertheless, this rather simple interpretation does not consider the heterogeneous tissue consolidation effects due to the juxtaposition of soft (CEP) and hard (BEP) tissue layers, which might have to be explored through micromechanical models of the BEP-CEP interface. Interstitial fluid velocity has been shown as an important mechanical stimuli for bone marrow stem cell differentiation[38] and chondrocyte mechano-sensing[39]. Our results can thus be significant for future studies aiming at more precise mechano-sensing estimations towards evolutionary predictions of the phenotypes of the stem cells present in the CEP[40].

It has been proposed that CEP calcification could affect the quantity of solute mass transported actively by fluid flow via hydraulic permeability changes[41]. However, it has also been shown *in vitro*[42] and *in silico*[43] that, compared to the diffusive transport, such *advective* transport of small solutes is negligible within the CEP. Because also BEP permeability variations played a negligible role on the concentration of solutes, we can anticipate that the advective transport of metabolites is unlikely to occur at the interface with the disc. Along with the predicted effect of limited diffusion with decreased fluid volume fraction[36], the above conclusion leaves two inter-related important aspects to tackle in order to understand the effective contribution of vertebral endplates to IVD nutrition: (1) effective blood supply and available solute concentration at the endplates (related to capillary openings) and (2) sources of modification of CEP porosity (i.e., trough calcification). Once addressed experimentally or clinically, these aspects might be further targeted through personalized, image-based multiphysics simulations to explore the relations among tissue structure, tissue function, and IVD biophysics.

Conclusive remarks

In summary, the present study explored separately the poromechanics of the osseous and the cartilaginous regions of the thin vertebral endplate, and provided tissue-specific quantifications of fluid-related parameters and their direct effect on disc maintenance. Important structural relationships between bone porosity and permeability were obtained and showed to pertain to universal relationships when compared to other measurements on different types of bone. Although the bony part of the endplate had a negligible effect on the disc metabolic transport prediction within the IVD, image-based values of bone parameters related to fluid flow could provide more realistic estimations of the mechanobiological stimuli sensed by cells from the endplates. Such outcomes can be particularly relevant to explore the calcification mechanisms of the BEP-CEP interface, also applied to regenerative and cell therapies, for which the maintenance or the restoration of the endplates is a major challenge[40].

Author contributions

AM collected, analyzed and interpreted the data, drafted the first version of the manuscript and performed the statistical analysis and simulations. DL, AM and JN designed the study. CH, KI and SJF offered technical support and analyzed and interpreted the data. DL, CH, KI and JN obtained the funding, designed the study, analyzed and interpreted the data and supported the statistical analysis.

All authors contributed in the critical revision of the article for important intellectual content and all authors approved the final manuscript.

Funding sources

This work was supported in part by the bilateral Austrian-Spanish Scientific Exchange grant ES 06/2010 AT2009-0029 between the Austrian Agency for International Cooperation in Education and Research and the Ministry of Economy and Competitiveness, as well as by the European Commission under the theme FP7-ICT-2009-6 of the seventh Framework Programme (Grant no. 269909, My SPINE).

Competing interest statement

The authors declare no competing interests.

Acknowledgements

The authors are grateful for the support of Prof Heinz Redl and Karl Kropik from the Ludwig Boltzmann Institute for Experimental and Clinical Traumatology, Vienna, Austria, in the framework of the Austrian Cluster for Tissue Regeneration.

Supplementary data

Supplementary data related to this article can be found at http://dx.doi.org/10.1016/j.joca.2014.05.005.

References

1. Roberts S, Menage J, Urban JP. Biochemical and structural properties of the cartilage end-plate and its relation to the intervertebral disc. Spine (Phila Pa 1976) 1989;14(2):166–74.
2. Taylor JR. Growth of human intervertebral discs and vertebral bodies. J Anat 1975;120(Pt 1):49–68.
3. Malko JA, Hutton WC, Fajman WA. An in vivo magnetic resonance imaging study of changes in the volume (and fluid content) of the lumbar intervertebral discs during a simulated diurnal load cycle. Spine (Phila Pa 1976) 1999;24(10):1015–22.
4. Ayotte DC, Ito K, Perren SM, Tepic S. Direction-dependent constriction flow in a poroelastic solid: the intervertebral disc valve. J Biomech Eng 2000;122(6):587–93.
5. Malandrino A, Planell JA, Lacroix D. Statistical factorial analysis on the poroelastic material properties sensitivity of the lumbar intervertebral disc under compression, flexion and axial rotation. J Biomech 2009;42(16):2780–8.

6. Urban JPG, Smith S, Fairbank JCT. Nutrition of the intervertebral disc. Spine (Phila Pa 1976) 2004;29(23):2700–9.
7. Benneker LM, Heini PF, Alini M, Anderson SE, Ito K. 2004 Young Investigator Award Winner: vertebral endplate marrow contact channel occlusions and intervertebral disc degeneration. Spine (Phila Pa 1976) 2005;30(2):167–73.
8. Luoma K, Riihimäki H, Luukkonen R, Raininko R, Viikari-Juntura E, Lamminen A. Low back pain in relation to lumbar disc degeneration. Spine (Phila Pa 1976) 2000;25(4):487–92.
9. Lee CR, Iatridis JC, Poveda L, Alini M. In vitro organ culture of the bovine intervertebral disc: effects of vertebral endplate and potential for mechanobiology studies. Spine (Phila Pa 1976) 2006;31(5):515–22.
10. Aigner T, Gresk-otter KR, Fairbank JC, Von Der Mark K, Urban JP. Variation with age in the pattern of type X collagen expression in normal and scoliotic human intervertebral discs. Calcif Tissue Int 1998;63(3):263–8.
11. Bernick S, Cailliet R. Vertebral end-plate changes with aging of human vertebrae. Spine (Phila Pa 1976) 1982;7(2):97–102.
12. Oda J, Tanaka H, Tsuzuki N. Intervertebral disc changes with aging of human cervical vertebra. From the neonate to the eighties. Spine (Phila Pa 1976) 1988;13(11):1205–11.
13. Nachemson A, Lewin T, Maroudas A, Freeman MA. In vitro diffusion of dye through the end-plates and the annulus fibrosus of human lumbar inter-vertebral discs. Acta Orthop Scand 1970;41(6):589–607.
14. Nguyen-minh C, Haughton VM, Papke RA, An H, Censky SC. Measuring diffusion of solutes into intervertebral disks with MR imaging and paramagnetic contrast medium. AJNR Am J Neuroradiol 1998;19(9):1781–4.
15. Holm S, Holm AK, Ekström L, Karladani A, Hansson T. Experimental disc degeneration due to endplate injury. J Spinal Disord Tech 2004;17(1):64–71.
16. Rodriguez AG, Slichter CK, Acosta FL, Rodriguez-Soto AE, Burghardt AJ, Majumdar S, *et al.* Human disc nucleus properties and vertebral endplate permeability. Spine (Phila Pa 1976) 2011;36(7):512–20.
17. Rajasekaran S, Babu JN, Arun R, Armstrong BRW, Shetty AP, Murugan S. ISSLS prize winner: a study of diffusion in human lumbar discs: a serial magnetic resonance imaging study documenting the influence of the endplate on diffusion in normal and degenerate discs. Spine (Phila Pa 1976) 2004;29(23):2654–67.
18. Gruber HE, Gordon B, Williams C, Norton HJ, Hanley EN. Vertebral endplate and disc changes in the aging sand rat lumbar spine: cross-sectional analyses of a large male and female population. Spine (Phila Pa 1976) 2007;32(23):2529–36.
19. Wang Y, Battié MC, Boyd SK, Videman T. The osseous endplates in lumbar vertebrae: thickness, bone mineral density and their associations with age and disk degeneration. Bone 2010:8–13.
20. Laffosse J-M, Accadbled F, Molinier F, Bonnevialle N, de Gauzy JS, Swider P. Correlations between effective permeability and marrow contact channels surface of vertebral endplates. J Orthop Res 2010;28(9):1229–34.
21. Malandrino A, Fritsch A, Lahayne O, Kropik K, Redl H, Noailly J, *et al.* Anisotropic tissue elasticity in human lumbar vertebra, by means of a coupled ultrasound-micromechanics approach. Mater Lett 2012;78:154–8.
22. Martin RB. Porosity and specific surface of bone. Crit Rev Biomed Eng 1984;10(3):179–222.
23. Cowin SC. Bone Mechanics Handbook. CRC Press; 2001.
24. Malandrino A, Noailly J, Lacroix D. The effect of sustained compression on oxygen metabolic transport in the intervertebral disc decreases with degenerative changes. PLoS Comput Biol 2011;7(8):e1002112.
25. Malandrino A, Lacroix D, Noailly J. Intervertebral disc cell death explained by metabolism-deformation couplings in a porohyperelastic finite element model. In: Poromechanics V, Ed. Proceedings of the Fifth Biot Conference on Poromechanics. Reston, VA: American Society of Civil Engineers; 2013:2193–201.
26. Beaudoin AJ, Mihalko WM, Krause WR. Finite element modelling of polymethylmethacrylate flow through cancellous bone. J Biomech 1991;24(2):127–36.
27. Grimm MJ, Williams JL. Measurements of permeability in human calcaneal trabecular bone. J Biomech 1997;30(7):743–5.
28. Hui PW, Leung PC, Sher A. Fluid conductance of cancellous bone graft as a predictor for graft-host interface healing. J Biomech 1996;29(1):123–32.
29. Nauman EA, Fong KE, Keaveny TM. Dependence of intertrabecular permeability on flow direction and anatomic site. Ann Biomed Eng 1999;27(4):517–24.
30. Dormieux L, Kondo D. Approche micromécanique du couplage perméabilité–endommagement. Comptes Rendus Mécanique 2004;332(2):135–40.
31. Vuong J, Hellmich C. Bone fibrillogenesis and mineralization: quantitative analysis and implications for tissue elasticity. J Theor Biol 2011;287(1):115–30.
32. Blanchard R, Dejaco A, Bongaers E, Hellmich C. Intravoxel bone micromechanics for microCT-based finite element simulations. J Biomech 2013;46(15):2710–21.
33. Widmer RP, Ferguson SJ. On the interrelationship of permeability and structural parameters of vertebral trabecular bone: a parametric computational study. Comput Methods Biomech Biomed Engin 2013;16(8):908–22.
34. Shirazi-Adl A, Taheri M, Urban JPG. Analysis of cell viability in intervertebral disc: effect of endplate permeability on cell population. J Biomech 2010;43(7):1330–6.
35. Jackson AR, Huang C-Y, Gu WY. Effect of endplate calcification and mechanical deformation on the distribution of glucose in intervertebral disc: a 3D finite element study. Comput Methods Biomech Biomed Engin 2011;14(2):195–204.
36. Malandrino A, Noailly J, Lacroix D. Numerical exploration of the combined effect of nutrient supply, tissue condition and deformation in the intervertebral disc. J Biomech 2014;47(6):1520–5.
37. Roberts S, Menage J, Eisenstein SM. The cartilage end-plate and intervertebral disc in scoliosis: calcification and other sequelae. J Orthop Res 1993;11(5):747–57.
38. Potier E, Noailly J, Ito K. Directing bone marrow-derived stromal cell function with mechanics. J Biomech 2010;43(5):807–17.
39. Degala S, Williams R, Zipfel W, Bonassar LJ. Calcium signaling in response to fluid flow by chondrocytes in 3D alginate culture. J Orthop Res 2012;30(5):793–9.
40. Liu L-T, Huang B, Li C-Q, Zhuang Y, Wang J, Zhou Y. Characteristics of stem cells derived from the degenerated human intervertebral disc cartilage endplate. PLoS One 2011;6(10):e26285.
41. Huang C-Y, Gu WY. Effects of mechanical compression on metabolism and distribution of oxygen and lactate in intervertebral disc. J Biomech 2008;41(6):1184–96.
42. Katz MM, Hargens AR, Garfin SR. Intervertebral disc nutrition: diffusion versus convection. Clin Orthop Relat Res 1986;210(210):243–5.
43. Ferguson SJ, Ito K, Nolte L-P. Fluid flow and convective transport of solutes within the intervertebral disc. J Biomech 2004;37(2):213–21.